Four molecular superconductors isolated as nanoparticles

Dominique de Caro,*[a,b] Christophe Faulmann,*[a,b] Lydie Valade,[a,b] Kane Jacob,[a,b] Imane Chtioui,[a,b] Soukaina Foulal,[a,b] Pascale de Caro,[c,d] Manon Bergez-Lacoste,[c,d] Jordi Fraxedas,[e] Belén Ballesteros,[e] James S. Brooks,[f] Eden Steven,[f] and Laurel E. Winter[f]

Keywords: nanoparticle / molecular superconductor / Bechgaard salts / $(TMTSF)_2X$ / ET_2I_3 / $TTF[Ni(dmit)_2]_2$

Abstract

$(TMTSF)_2PF_6$ and $(TMTSF)_2ClO_4$ Bechgaard salts, $(BEDT\text{-}TTF)_2I_3$, and $TTF[Ni(dmit)_2]_2$ are among the most popular molecular superconductors. They are grown as nanoparticles exhibiting properties in agreement with those of bulk. The shape, size and homogeneity of particles depend on the stabilizing agent and synthesis conditions. We report on the more recent conditions investigated (i) to produce nanoparticles of 35 nm for β-$(BEDT\text{-}TTF)_2I_3$, (ii) to reduce the particles size down to 10-15 nm for $TTF[Ni(dmit)_2]_2$, and 3-5 nm for $(TMTSF)_2ClO_4$, and (iii) to improve the growth duration from days to 1h for $(TMTSF)_2PF_6$. Finally, we report on superconductivity evidence in $(TMTSF)_2ClO_4$ particles.

Introduction

The four molecular superconductors $(TMTSF)_2PF_6$ and $(TMTSF)_2ClO_4$, $(BEDT\text{-}TTF)_2I_3$, and $TTF[Ni(dmit)_2]_2$ (Scheme 1) were first prepared in the 1980's and 1990's.[1] They are the parent compounds of well-known series of superconductors and can be taken as models for studying the influence of morphology and size on physical properties, for instance on the occurrence of superconductivity. We have explored the preparation of these compounds as thin films[1] and as nanoparticles (NPs).[2] $(BEDT\text{-}TTF)_2I_3$ was also studied as composite films.[3] In particular, superconductivity was evidenced in thin films of $TTF[Ni(dmit)_2]_2$,[4] $(TMTSF)_2ClO_4$[5] and $(BEDT\text{-}TTF)_2I_3$.[6] Preparing molecular conductors as thin films or nanoparticles follows the ultimate goal to integrate them into electronic devices. In this case, the materials are selected for their room-temperature properties. Therefore, research focus on their preparation in forms transferable onto surfaces, and on the study of the consequences of the final morphology on physical properties. For example, colloidal solutions of TTF-TCNQ NPs offer promising applications,[7] a chemistry-based technique for patterning films of $(BEDT\text{-}TTF)_2I_3$ on a polymeric substrate was described,[8] and surface selective deposition of TTF-TCNQ, $TTF[Ni(dmit)_2]_2$ and $(BEDT\text{-}TTF)_2I_3$ NPs was applied for building organic transistor structures.[2b]

Taking advantage of our previous work, we investigated the preparation of NPs of β-$(BEDT\text{-}TTF)_2I_3$ and developed new conditions of preparation of NPs of $TTF[Ni(dmit)_2]_2$, $(TMTSF)_2PF_6$ and $(TMTSF)_2ClO_4$, in order to produce smaller homogeneous particles (Table 1) and perform their physical studies to evidence superconductivity. We report the preparation and study of NPs of β_{CO}-$(BEDT\text{-}TTF)_2I_3$ (CO stands for "chemical oxidation") obtained following an iodine chemical oxidation of BEDT-TTF[1, 9] in presence of the ionic liquid (IL) $(BMIM)[N(CF_3SO_2)_2]$ (Scheme 2). We describe the preparation of $TTF[Ni(dmit)_2]_2$ NPs at room temperature using an electrochemical procedure in presence of $(BMIM)[N(CF_3SO_2)_2]$. $(TMTSF)_2PF_6$ and $(TMTSF)_2ClO_4$ NPs are prepared by electrolysis as previously reported.[2a] In this work, we investigate the influence of the growth speed on size and morphology of $(TMTSF)_2PF_6$ NPs, and of the addition of neutral long chain molecules to the ammonium salts *n*-Bu_4NClO_4 and $[Me(n\text{-}Oct)_3N]ClO_4$ on the formation of $(TMTSF)_2ClO_4$ NPs. Finally, we present the preliminary physical studies that show the occurrence of superconductivity in $(TMTSF)_2ClO_4$ NPs.

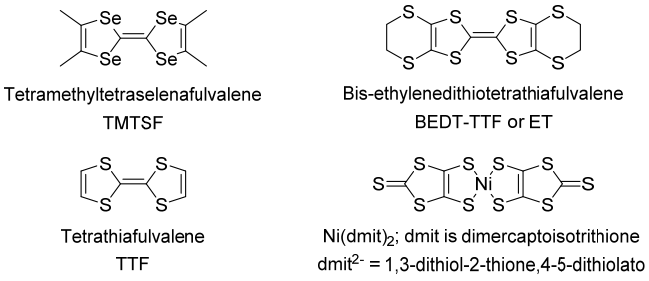

Scheme 1. Molecular building blocks of $(TMTSF)_2PF_6$, $(TMTSF)_2ClO_4$, $(BEDT\text{-}TTF)_2I_3$, and $TTF[Ni(dmit)_2]_2$ superconductors.

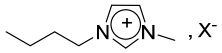

1-butyl-3-methylimidazolium
$BMIM^+$; $X^- = BF_4^-$, $[N(CF_3SO_2)_2]^-$

Scheme 2. Ionic liquids used for growth control of nanoparticles

Table 1. Synthesis conditions of β_{CO}-(BEDT-TTF)$_2$I$_3$, TTF[Ni(dmit)$_2$]$_2$, (TMTSF)$_2$PF$_6$ and (TMTSF)$_2$ClO$_4$ nanoparticles. All experiments have been performed at room temperature, following electrochemical procedures, unless otherwise specified (see experimental section for details)..

Precursors and Stabilisers	Solvent	Current intensity Duration	NPs characteristics
BEDT-TTF I_2 (BMIM)[$N(CF_3SO_2)_2$]	THF	Chemical procedure at 85°C	NPs 35 nm
TTF *n*-Bu$_4$N[Ni(dmit)$_2$] (BMIM)BF$_4$	CH_3CN	150 µA / 24h	NPs 15-20 nm
TTF *n*-Bu$_4$N[Ni(dmit)$_2$] (BMIM)[$N(CF_3SO_2)_2$]	CH_3CN	80 µA / 24h	Nanosticks 15-20 nm
TTF *n*-Bu$_4$N[Ni(dmit)$_2$] (BMIM)[$N(CF_3SO_2)_2$]	CH_3CN	500 µA / 4h	NPs 10-15 nm
TMTSF (BMIM)PF$_6$	CH_2Cl_2	10 µA / 72h	NPs 30-50 nm
TMTSF (BMIM)PF$_6$	CH_2Cl_2	200 µA 3h50	NPs 50 nm
TMTSF (BMIM)PF$_6$	CH_2Cl_2	500 µA 1h15	NPs 55 nm
TMTSF [Me(*n*-Oct)$_3$N]ClO$_4$	CH_2Cl_2	10 µA / 3d	NPs 25-35 nm
TMTSF *n*-Bu$_4$NClO$_4$ hexadecylamine	THF	10 µA / 3d	NPs 35 nm
TMTSF *n*-Bu$_4$NClO$_4$ dodecylamine	THF	10 µA / 3d	NPs 40-65 nm
TMTSF *(n*-Bu4N*)*ClO$_4$ *n*-octylamine	THF	10 µA / 3d	NPs 35-70 nm
TMTSF *n*-Bu$_4$NClO$_4$ methyloleate	THF	10 µA / 3d	NPs 20-60 nm
TMTSF *n*Bu$_4$NClO$_4$ N-octylfurfurylimine	THF	10 µA / 3d	NPs 20-60 nm
TMTSF *n*-Bu$_4$NClO$_4$ N-octylfuran-2-carboxamide	THF	10 µA / 3d	NPs 20-60 nm
TMTSF [Me(*n*-Oct)$_3$N]ClO$_4$ hexadecylamine	CH_2Cl_2	40 µA / 20h	NPs 20-50 nm

Results and Discussion

β_{CO}-(BEDT-TTF)$_2$I$_3$ nanoparticles

BEDT-TTF afforded the largest number of superconducting phases exhibiting various structural arrangements depending on the associated anions. The superconductor (BEDT-TTF)$_2$I$_3$ can adopt the three well-known β-, θ-, and κ-type modifications.[1, 10] All of them show superconducting transitions at ambient pressure.[11] Nanocrystals of α- and β-(BEDT-TTF)$_2$I$_3$ were observed in thin films as imbedded in a polycarbonate matrix[12] and in core-shell-type nanocomposite NPs of α-(BEDT-TTF)$_2$I$_3$ where the nanocrystals act as shell layers and as the binder in aggregated silica particles.[13] Core-shell well-dispersed NPs consisting of the molecular conductor as the core material and the stabilizing agent as the shell layer can be isolated by using appropriate stabilizing agents. Polyvinylpyrrolidone (PVP) (Scheme 3) was

successfully used to prepare NPs of $(BEDT\text{-}TTF)_2I_3$.[2b] We have investigated the use of the ionic liquid (IL) $(BMIM)[N(CF_3SO_2)_2]$ as the stabilizing agent.

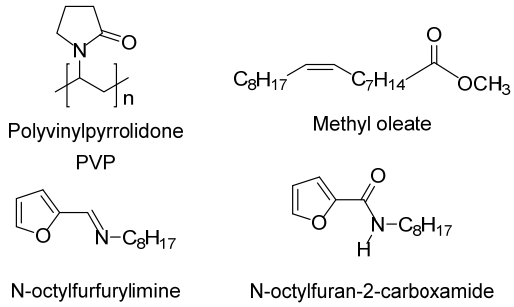

Scheme 3. Polymers used for growth control of nanoparticle

β_{CO}-$(BEDT\text{-}TTF)_2I_3$ NPs are prepared by chemical oxidation of BEDT-TTF by iodine, using a procedure previously reported.[1, 9] and in presence of $(BMIM)[N(CF_3SO_2)_2]$ Compared to previously isolated nanomaterials based on $(BEDT\text{-}TTF)_2I_3$, this procedure affords well-dispersed NPs with an average size of 35 nm as observed by TEM (Figure 1). X-Ray diffraction, Raman and IR spectroscopies confirm the formation of β_{CO}-$(BEDT\text{-}TTF)_2I_3$ (see Sup. Mat., Figures S1-S3). The room temperature conductivity of the NPs powder, measured on a compacted pellet, is 1.5 $S.cm^{-1}$. This value is consistent with the respective contributions to the conductivity: intrinsic conductivity of NPs, resistance due to the IL shell around NPs, and Nps boundaries.

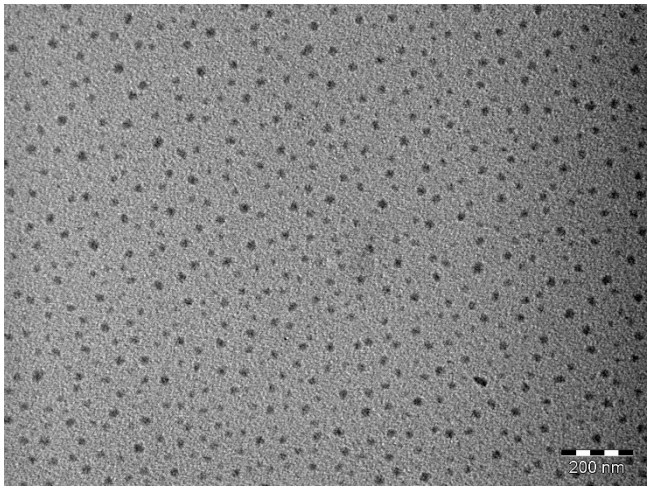

Figure 1. Electron micrographs for β_{CO}-$(BEDT\text{-}TTF)_2I_3$ with $(BMIM)[N(CF_3SO_2)_2]$; scale bar = 200 nm.

$TTF[Ni(dmit)_2]_2$ nanoparticles

The $[Ni(dmit)_2]$ molecule afforded the first series of superconductors containing a transition metal complex as the acceptor building block. The series opened with the $TTF[Ni(dmit)_2]_2$ compound exhibiting a room temperature conductivity of 300 $S.cm^{-1}$ and a Tc at 1.6 K under an applied hydrostatic pressure of 7 kbar[14]. The phase diagram of this compound was additionally investigated recently.[15] The preparation of thin films, nanowires and nanoparticles of $TTF[Ni(dmit)_2]_2$ was investigated[16] and superconductivity was evidenced in electrodeposited films.[4] Previously synthesised NPs of $TTF[Ni(dmit)_2]_2$ were prepared using a chemical procedure involving the reaction of $(TTF)_3(BF_4)_2$ with *n*-$Bu_4N[Ni(dmit)_2]$.[2a, 16b] The best results in terms of shape, dispersion and homogeneity of the NPs were obtained in the presence of

(BMIM)BF_4 or (BMIM)[$N(CF_3SO_2)_2$] and at -80 °C. These conditions afford particles of 30 nm (Figure 2a). When this chemical procedure is conducted at room temperature, less NPs are produced and they are irregular, aggregated or elongated. When TTF is electrochemically oxidised in presence of *n*-Bu_4N[$Ni(dmit)_2$] and either (BMIM)BF_4 or (BMIM)[$N(CF_3SO_2)_2$], well-dispersed NPs of TTF[$Ni(dmit)_2]_2$ are produced at room temperature. TEM observations show nanoparticles of 15-20 nm and 10-15 nm in (BMIM)BF_4 and (BMIM)[$N(CF_3SO_2)_2$], respectively (Figure 2b and 2c). The electrochemical procedure affords nanoparticles at room temperature with smaller size than the chemical procedure. Additionally, the process is more efficient to produce nanoparticles at high current density: nanosticks are preferred when the electrolysis is conducted for 24h at 80 μA and nanoparticles are obtained at 500 μA for 4h. IR and Raman spectroscopies confirm the formation of TTF[$Ni(dmit)_2]_2$ (see Sup. Mat., Figures S4, S5). The conductivity was measured on a compacted pellet of NPs powder and found to be 0.5 $S.cm^{-1}$ consistent with powdered samples.

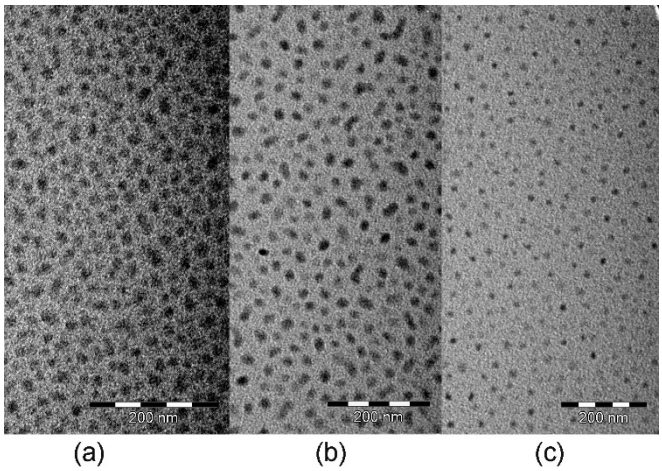

Figure 2. Electron micrographs for TTF[$Ni(dmit)_2]_2$ with (a) Chemical procedure, (BMIM)BF_4, -80°C (b) electrochemical procedure, (BMIM)BF_4, (c) electrochemical procedure, (BMIM)[$N(CF_3SO_2)_2$]; scale bar = 200 nm.

$(TMTSF)_2PF_6$ nanoparticles

$(TMTSF)_2PF_6$ belongs to the so-called Bechgaard salts that led to the first organic superconducting phases. $(TMTSF)_2PF_6$ undergoes a superconductive transition at 0.9K under a pressure of 12 kbar.[17] NPs of $(TMTSF)_2PF_6$ have previously been isolated by electrolysis in presence of (BMIM)PF_6 that acts as both the supporting electrolyte and the stabiliser.[18] We have followed similar concentration conditions (TMTSF/IL = 1/10) and have investigated the influence of the current intensity on the shape and size of NPs. The electrolysis is conducted at constant current. The anodic compartment solution being stirred, the NPs formed on the electrode fall down and the electrode surface can be considered as unchanged during the process; therefore, the growth speed is directly proportional to the current intensity. In these conditions, the higher the current, and the higher the growth speed. At 10 μA, the electrolysis is conducted for 3 days: the particles morphology is uniform but their size ranges from 30 nm to 50 nm. When the current is fixed at 200 μA, the electrolysis is stopped after 3h50 and all particles are in the 50 nm size range. Almost the same size is obtained (55 nm) at a current of 500 μA applied for 1h15 (Figure 3).

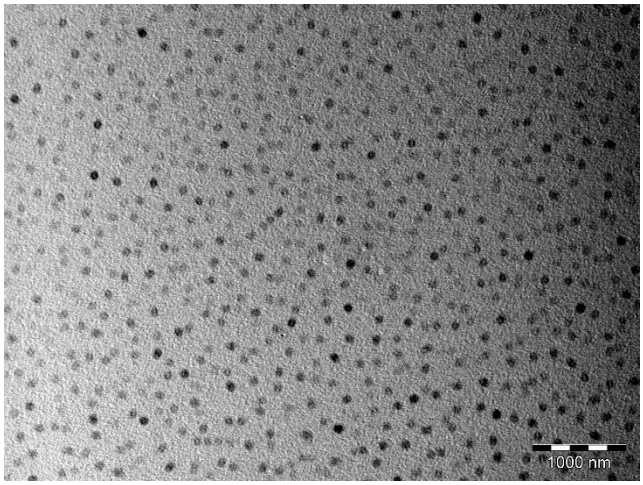

Figure 3. Electron micrograph for $(TMTSF)_2PF_6$ with $(BMIM)PF_6$ at 500 μA; scale bar = 1000 nm.

Well-dispersed and homogeneous NPs can therefore be readily prepared at currents ranging from 200 μA and 500 μA. IR spectrum (Figure S6 in Sup. Mat.) is identical for the particles grown in these conditions as those previously grown.[18]

$(TMTSF)_2ClO_4$ nanoparticles

$(TMTSF)_2ClO_4$ was the first organic superconductor at ambient pressure with a Tc at 1.3 K.[19] As for $(TMTSF)_2PF_6$, NPs of $(TMTSF)_2ClO_4$ have previously been isolated by electrolysis in presence of the long chain ammonium salt $[Me(n\text{-}Oct)_3N]ClO_4$, acting as both the supporting electrolyte and the stabiliser.[2a, 18] We have investigated their preparation in presence of $n\text{-}Bu_4NClO_4$ or $[Me(n\text{-}Oct)_3N]ClO_4$ as the supporting electrolyte and neutral long chain molecules as the stabilisers (Table 1, Scheme 3). Except for hexadecylamine, whatever the neutral amphiphilic molecule, TEM micrographs exhibit similar features: nanocrystals with sizes in the 20-70 nm range (Figure 4).

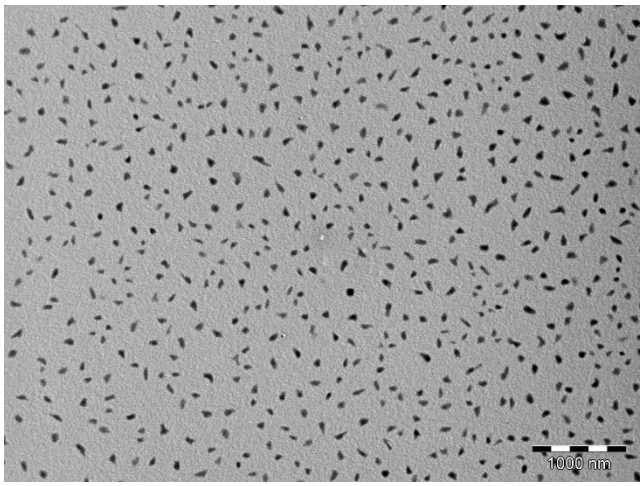

Figure 4. Electron micrographs for $(TMTSF)_2ClO_4$ with octylamine and $n\text{-}Bu_4NClO_4$; scale bar = 1000 nm.

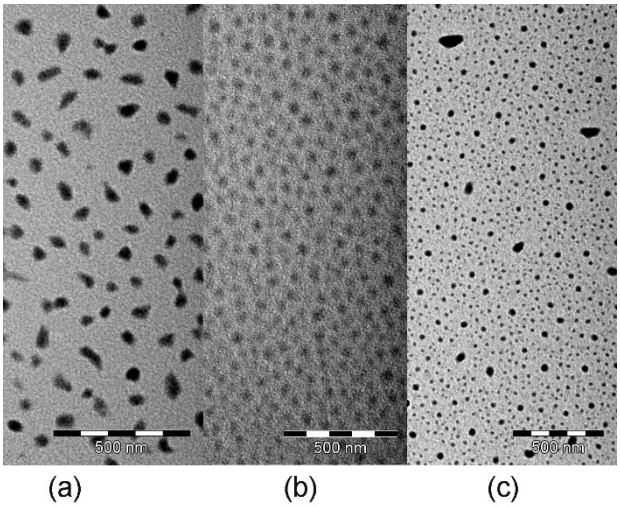

Figure 5. Electron micrographs for $(TMTSF)_2ClO_4$ with (a) $[Me(n\text{-}Oct)_3N]ClO_4$ (b) hexadecylamine and $n\text{-}Bu_4NClO_4$ (c) hexadecylamine and $[Me(n\text{-}Oct)_3N]ClO_4$ (all scale bars are 500 nm)

Similar nanocrystals have previously been observed when $(TMTSF)_2ClO_4$ is grown with $[Me(n\text{-}Oct)_3N]ClO_4$ (Figure 5a).[18] Nevertheless, in presence of the longer alkyl chain amine (hexadecylamine), spherical 35 nm diameter nanoparticles are obtained (Figure 5b). When hexadecylamine is used in combination with $[Me(n\text{-}Oct)_3N]ClO_4$, also bearing a long alkyl chain, smaller spherical NPs are observed together with few remaining nanocrystals (Figure 5c). A major improvement issues from these conditions: stable dispersions of NPs (*ca.* 1 day) can be prepared in acetonitrile (2-3 mg/mL).

HRTEM measurements performed at 200 kV (Figure 6) indicate that the 20-60 nm features observed in the lower-resolution TEM images from Figure 5a are in fact agglomerates of smaller NPs, with diameters in the 3-5 nm range. The observed interplanar spacings can be indexed in the vast majority of cases according to the well-known $(TMTSF)_2ClO_4$ triclinic crystal structure, indicating their high degree of order (see also Figure S6 in Sup. Mat.).

IR and Raman spectroscopies (see Figures S7 and S8 in Sup. Mat.) are identical for the particles grown in this medium as those previously grown.[18]

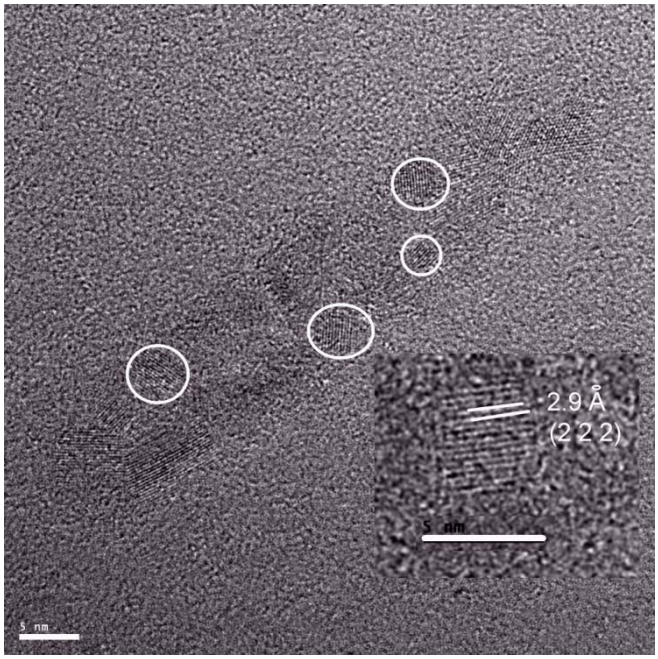

Figure 6. HRTEM image taken at 200 kV of aggregated NPs of $(TMTSF)_2ClO_4$ with $[Me(n\text{-}Oct)_3N]ClO_4$ exhibiting diameters in the 3-5 nm range (scale bar 5 nm) (insert: one indexed 4.5 nm NP)

Figure 7 shows high resolution XPS spectra of neutral TMTSF pressed microcrystalline powder (grey line) compared to pressed powder of $(TMTSF)_2ClO_4$ nanoparticles (short dotted line), respectively. The binding energy of the Se $3d_{5/2}$ line corresponding to neutral TMTSF is located at 55.6 eV, after correction of surface charge due to the insulating character of TMTSF. The Se $3d_{5/2}$-Se $3d_{3/2}$ doublet can be fitted to a mixed Gaussian-Lorentzian function with a FWHM of 0.9 eV, a branching ratio of 0.83 and a splitting of 0.9 eV, after a Shirley-type background subtraction. The Se 3d line corresponding to $(TMTSF)_2ClO_4$ can be decomposed into four contributions (dotted black lines) whose sum is represented as a black line and mimics the experimental data. In the fit, the values obtained for neutral TMTSF have been taken as fixed parameters in order to reduce the number of variables. No surface charge was detected indicating the conductive character of the powder. The resulting binding energies for the Se $3d_{5/2}$ components are 55.7, 56.1, 57.0 and 58.8 eV, respectively. The first one corresponds to TMTSF in the neutral state while the rest correspond to different oxidation states of TMTSF, evidencing charge transfer. The observed energy difference between the first two components, 0.4 eV, is characteristic of related molecules and has been found *e. g.*, in TTF on Au(111) surfaces corresponding to a total charge transfer of 0.3 electrons per molecule.[20] The same effect has been also observed for microcrystals of the closely-related Fabre salt $(TMTTF)_2PF_6$ [TMTTF = tetramethyltetrathiafulvalene]. In this case two equally intense S2p components separated by about 1 eV have been reported corresponding to both the neutral and charged (+1) configurations.[21] Analogous S2p spectra have been obtained for TTF-TCNQ single crystals, with two components separated by *ca.* 1 eV (about 0.6 charge transfer).[22] The reason behind the observation of different configurations is that photoemission is a rapid process (in the 10^{-15} s range). The components associated to the salt appear broader (1.1 eV FWHM) than for TMTSF (0.9 eV FWHM) due to the small size of the nanoparticles as compared to the microcrystalline size of neutral TMTSF. The small size is possibly responsible for the presence of more than two oxidation states (neutral and +1) for $(TMTSF)_2ClO_4$ nanoparticles. On the other hand, Raman spectroscopy (Figure S8) evidences the $\nu_4(a_g)$ mode of the central C=C bond of TMTSF at 1461 cm^{-1}, confirming the expected +0.5 formal charge for TMTSF in $(TMTSF)_2ClO_4$.[23]

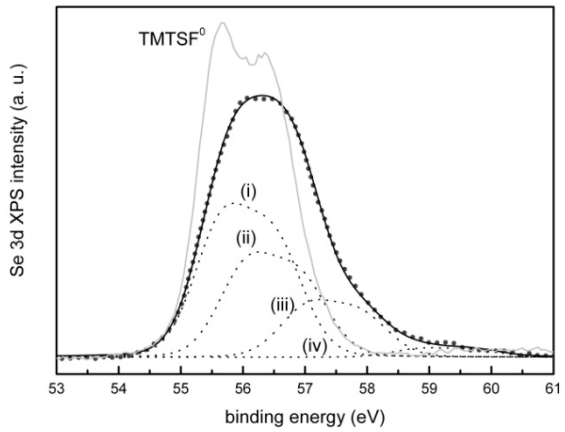

Figure 7. XPS spectra of $(TMTSF)_2ClO_4$ (short dotted line: experimental: black line:calculated) and TMTSF (grey line); the four black dotted lines (from (i) to (iv)) correspond to the deconvolution of the black line (see text for details of the fit).

To measure the superconducting properties of $(TMTSF)_2ClO_4$ NPs, we performed inductive magnetic susceptibility measurements using a tunnel diode oscillator (TDO) (Figure 8). The sample was slow cooled between 40 K and 15 K at a rate of approximately 0.05 K/min to ensure the anion ordering took place and the material would be in the superconducting state. Afterwards we monitored the frequency from 1.4 K to 0.031 K as the dilution refrigerator cooled down and warmed up, which took about 8.3 hours each to complete. Results are shown as negative frequency due to frequency change being proportional to the negative change of magnetic susceptibility. As a result, Figure 8 shows a decrease in negative frequency as the material undergoes the superconducting transition, as expected. The black curve (right axis) is relative susceptibility versus temperature for a bundle of $(TMTSF)_2ClO_4$ crystals[24] that shows a similar change in susceptibility through the superconducting transition. Isothermal magnetic field sweeps below Tc (~ 1.2 K) show a type II critical field behavior that is also consistent with the results of ref. [24]. These results will be reported elsewhere.[25]

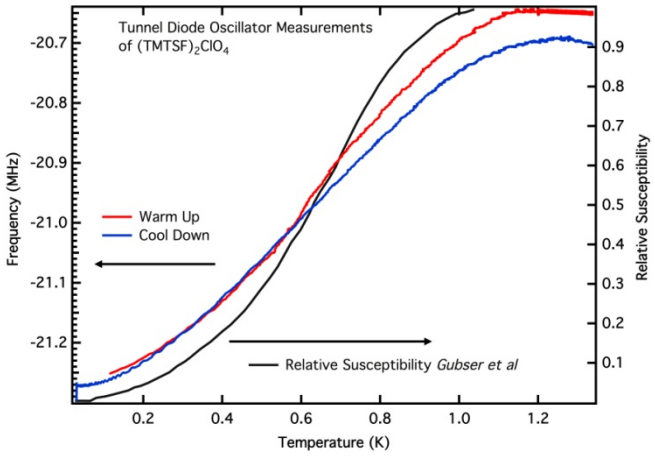

Figure 8. Observation of the superconducting transition of nanoparticles of $(TMTSF)_2ClO_4$ as a function of temperature using a TDO (left axis, blue and red curves).

Conclusions

The preparation of nanoparticles of the four molecular superconductors β-$(BEDT\text{-}TTF)_2I_3$, $TTF[Ni(dmit)_2]_2$, $(TMTSF)_2PF_6$, and $(TMTSF)_2ClO_4$, was successfully performed in various conditions to answer multiple goals: (i) preparing new examples of nanoparticles as

the well-dispersed NPs of β-(BEDT-TTF)$_2$I$_3$ with an average size of 35 nm, (ii) reducing the particle size by applying an electrochemical method for growing, at room temperature, 10-15 nm NPs of TTF[Ni(dmit)$_2$]$_2$, (iii) producing higher amounts of homogeneous particles in quicker time (1h *vs.* days) in the case of (TMTSF)$_2$PF$_6$, and (iv) evidencing the superconducting transition at low particle size for NPs of (TMTSF)$_2$ClO$_4$. Conditions are now available for isolating these systems as spherical uniform particles, a challenge in the field of molecular conductors and superconductors that preferably grow as needles. We have additionally evidenced that spherical crystalline nanoparticles of (TMTSF)$_2$ClO$_4$ as small as 3-5 nm can be formed, organise as 20-60 nm nanocrystals, and exhibit the superconducting transition observed on macroscopic single crystals. Further physical studies of NPs of (TMTSF)$_2$ClO$_4$ and other molecular superconductors are under progress to figure out the mechanism explaining the occurrence of superconductivity at such a small size.

Experimental Section

Synthesis: All syntheses are performed at room temperature under argon atmosphere, except the synthesis of β_{CO}-(BEDT-TTF)$_2$I$_3$. Solvents (tetrahydrofurane, acetonitrile and methylene chloride) are distilled and stored under argon prior to use. BEDT-TTF, TTF, TMTSF, octylamine, dodecylamine, hexadecylamine, methyloleate, *n*-Bu$_4$NClO$_4$ and (BMIM)X (X = [N(CF$_3$SO$_2$)$_2$], BF$_4$, PF$_6$) are commercially available and used as received. [Me(*n*-Oct)$_3$N]ClO$_4$ and *n*-Bu$_4$N[Ni(dmit)$_2$] are prepared as described in refs. [18] and [26], respectively. N-octylfuran-2-carboxamide and N-octylfurfurylimine are prepared following procedures described in ref. [27].

β_{CO}-(BEDT-TTF)$_2$I$_3$ nanoparticles: 100 mg of BEDT-TTF and 1.5 mL of (BMIM)[N(CF$_3$SO$_2$)$_2$] are dissolved in 60 mL of THF. A solution of 99 mg of I$_2$ in 20 mL of THF is added dropwise over 1h to the first solution heated at 85 °C. The reaction mixture is further cooled down to room temperature and for 1h at 0°C. 160 mg of a shiny black precipitate is collected by filtration and dried under vacuum for 4h.

General conditions of electrosynthesis of nanoparticles: the synthesis is performed in a classical H-shaped electrocrystallization cell equipped with two platinum wire electrodes (L = 1 cm, d = 1 mm).[28] The anodic and cathodic compartments are filled with a solution of the selected stabilizing medium (ionic liquid, amine, ammonium salt, from 3 to 10 eq./TTF or TMTSF) and the appropriate supporting electrolyte. The donor molecule (TTF, TMTSF) is placed in the anodic compartment. The electrolysis is conducted at room temperature under galvanostatic conditions. The anodic solution is vigorously stirred all along the electrolysis duration. The air stable black powders of NPs are collected by filtration from the anodic compartment.

TTF[Ni(dmit)$_2$]$_2$ nanoparticles: the anodic compartment contains 12 mg of TTF, 81 mg of *n*-Bu$_4$N[Ni(dmit)$_2$] and 90 µL of (BMIM)[N(CF$_3$SO$_2$)$_2$] or (BMIM)BF$_4$ dissolved in 12 mL of acetonitrile. The cathodic compartment contains 90 µL of (BMIM)[N(CF$_3$SO$_2$)$_2$] or (BMIM)BF$_4$ dissolved in 12 mL of acetonitrile. The electrolysis is conducted at 150 µA for 24h in presence of (BMIM)BF$_4$ and at 80 µA for 24h and 500 µA for 4h in presence of (BMIM)[N(CF$_3$SO$_2$)$_2$].

(TMTSF)$_2$PF$_6$ nanoparticles: the anodic compartment contains 25 mg of TMTSF, and 90 mg of (BMIM)PF$_6$ dissolved in 12 mL of CH$_2$Cl$_2$. The cathodic compartment contains 90 mg of (BMIM)PF$_6$ dissolved in 12 mL of CH$_2$Cl$_2$. The electrolysis is conducted at different current densities and duration from 10 µA for 3 days to 500 µA for 1h15.

(TMTSF)$_2$ClO$_4$ nanoparticles: the anodic compartment contains 25 mg of TMTSF, and 80 mg of *n*-Bu$_4$NClO$_4$ or 105 mg of [Me(*n*-Oct)$_3$N]ClO$_4$ dissolved in 12 mL of solvent (CH$_2$Cl$_2$ or THF). The cathodic compartment contains 75 mg of *n*-Bu$_4$NClO$_4$ or 105 mg of [Me(*n*-Oct)$_3$N]ClO$_4$ dissolved in 12 mL of solvent. The following amphiphilic molecules are added to the anodic compartment: 32 mg of hexadecylamine or 25 mg of dodecylamine or 74 µL of *n*-octylamine, or 65 µL of methyloleate, or 37 mg of N-octylfuran-2-carboxamide, or 37 µL of N-octylfurfurylimine. Currents and durations of electrolysis are indicated in Table 1.

Physical measurements:

TEM experiments are performed on a JEOL Model JEM 1011 operating at 100 kV. Powder (0.5 mg) is dispersed in diethylether (2 mL) under slow stirring for 1 min. The TEM specimen is then prepared by evaporation of droplets of suspension deposited on carbon-supported copper grids.

HRTEM images were recorded using a FEI Tecnai F20 HRTEM operated at 200 kV. The samples were sonicated and dispersed in acetonitrile and placed dropwise onto a holey carbon copper support grid for HRTEM observation.

Ex-situ XPS experiments were performed at room temperature with a SPECS PHOIBOS 150 hemispherical analyzer at 10 eV pass energy using monochromatic Al K_α (1486.6 eV) radiation as excitation source in a base pressure of 10^{-9} mbar.

The tunnel diode oscillator (TDO) technique consists of an LC tank-circuit which oscillates at its resonant frequency $f_0 = (2\pi \text{ sqrt}(LC))^{1/2}$, and a tunnel diode that compensates for losses in the circuit. The sample to be studied goes inside of the inductor (L) coil and we monitor the change in frequency as a function of temperature and field. As the magnetic properties of the material changes, the effective inductance of the coil changes and therefore the resonant frequency of circuit changes, which we use as a measure of the magnetic susceptibility changes of the sample. In our experiment we packed 7.385 mg of the nanoparticle $(TMTSF)_2ClO_4$ inside of a plastic non-magnetic capsule which had an approximate volume of 22.51 mm^3. The capsule was then placed inside a 40 turn (L) coil of about 4.66 mm in length with an approximate volume of 26.73 mm^3. The resonant frequency was around 15 MHz and was mixed with a local 5 MHz frequency source to obtain the 20 – 21 MHz results presented in Figure 8. The experiment was run in a dilution refrigerator where temperature sweeps were carried out between 35 mK and 1.2 K, with a field range of -2 T to 2 T provided by a superconducting magnet.

Acknowledgements

Work done at the NHMFL is supported by NSF DMR-1309146 (JSB). The NHMFL is supported by NSF Cooperative Agreement No. DMR-1157490, the State of Florida, and the U.S. Department of Energy. Collaboration within the European Associated Laboratory Trans-Pyrénéen (LEA): “de la Molécule aux Matériaux” is appreciated. Work done at LCC is supported by the Centre National de la Recherche Scientifique (CNRS, France). I. C. thanks the MESR (Ministère de l’Enseignement Supérieur et de la Recherche) for a Ph.D grant.

Supporting Information (see footnote on the first page of this article): … . Various characterizations can be found in the Supplementary Information: Raman spectra for $(BEDT\text{-}TTF)_2I_3$, $TTF[Ni(dmit)_2]_2$ and $(TMTSF)_2ClO_4$; Infrared spectra for $(BEDT\text{-}TTF)_2I_3$, $TTF[Ni(dmit)_2]_2$, $(TMTSF)_2ClO_4$ and $(TMTSF)_2PF_6$; X-ray diffraction diagram for $(BEDT\text{-}TTF)_2I_3$ and HRTEM micrograph for $(TMTSF)_2ClO_4$.

[1] L. Valade, H. Tanaka, in *Molecular Materials* (Eds.: D. W. Bruce, R. Walton), John Wiley & Sons Ltd, **2010**, pp. 215-290.

[2] a) D. de Caro, L. Valade, C. Faulmann, K. Jacob, D. Van Dorsselaer, I. Chtioui, L. Salmon, A. Sabbar, S. El Hajjaji, E. Perez, S. Franceschi, J. Fraxedas, *New. J. Chem.* **2013**, *37*, 3331-3336; b) T. Kadoya, D. de Caro, K. Jacob, C. Faulmann, L. Valade, T. Mori, *J. Mater. Chem.* **2011**, *21*, 18421-18424.

[3] E. Laukhina, J. Ulanski, A. Khomenko, S. Pesotskii, V. Tkatchev, L. Atovmyan, E. Yagubskii, C. Rovira, J. Veciana, J. Vidal-Gancedo, V. Laukhin, *J. Phys. I France* **1997**, *7*, 1665-1675.

[4] J. P. Savy, D. De Caro, L. Valade, J. P. Legros, P. Auban-Senzier, C. R. Pasquier, J. Fraxedas, F. Senocq, *Europhys. Lett.* **2007**, *78*.

[5] J.-P. Savy, D. de Caro, L. Valade, J.-C. Coiffic, E. S. Choi, J. S. Brooks, J. Fraxedas, *Synth. Met.* **2010**, *160*, 855-858.

[6] E. E. Laukhina, V. A. Merzhanov, S. I. Pesotskii, A. G. Khomenko, E. B. Yagubskii, J. Ulanski, M. Kryszewski, J. K. Jeszka, *Synth. Met.* **1995**, *70*, 797-800.

[7] D. de Caro, M. Souque, C. Faulmann, Y. Coppel, L. Valade, J. Fraxedas, O. Vendier, F. Courtade, *Langmuir* **2013**, *29*, 8983–8988.

[8] M. Mas-Torrent, E. E. Laukhina, V. Laukhin, C. M. Creely, D. V. Petrov, C. Rovira, J. Veciana, *J. Mater. Chem.* **2006**, *16*, 543-545.

[9] a) E. É. Kostyuchenko, É. B. Yagubskii, O. Y. Neiland, V. Y. Khodorkovskii, *Russ Chem Bull* **1984**, *33*, 2598; b) E. E. Laukhina, V. N. Laukhin, A. G. Khomenko, E. B. Yagubskii, *Synth. Met.* **1989**, *32*, 381-388; c) H. Müller, S. O. Svensson, A. N. Fitch, M. Lorenzen, D. G. Xenikos, *Adv. Mat.* **1997**, *9*, 896-900.

[10] R. P. Shibaeva, E. B. Yagubskii, *Chem. Rev.* **2004**, *104*, 5347-5378.

[11] E. B. Yagubskii, I. F. Shchegolev, V. N. Laukhin, P. A. Kononovich, M. V. Karatsovnik, A. V. Zvarykina, L. I. Buravov, *Jetp Letters* **1984**, *39*, 12-16.

[12] A. Tracz, J. K. Jeszka, A. Sroczynska, J. Ulanski, T. Pakula, *Advanced Materials for Optics and Electronics* **1996**, *6*, 335-342.

[13] A. Funabiki, H. Sugiyama, T. Mochida, K. Ichimura, T. Okubo, K. Furukawa, T. Nakamura, *Rsc Advances* **2012**, *2*, 1055-1060.

[14] L. Brossard, M. Ribault, M. Bousseau, L. Valade, P. Cassoux, *Comptes Rendus de l'Académie des Sciences* **1986**, *302-II*, 205-210.

[15] W. Kaddour, P. Auban-Senzier, C. Pasquier, L. Valade, *Physica B-Condensed Matter* **2012**, *407*, 1715-1717.

[16] a) D. de Caro, J. Fraxedas, C. Faulmann, I. Malfant, J. Milon, J. F. Lamère, V. Collière, L. Valade, *Adv. Mat.* **2004**, *16*, 835-838; b) D. de Caro, K. Jacob, C. Faulmann, L. Valade, L. Viau, *Comptes Rendus Chimie* **2012**, *15*, 950-954.

[17] D. Jérome, A. Mazaud, M. Ribault, K. Bechgaard, *J. Physique Lett.* **1980**, *41*, 95-98.

[18] D. de Caro, K. Jacob, C. Faulmann, L. Valade, *Comptes Rendus Chimie* **2013**, *16*, 629-633.

[19] K. Bechgaard, K. Carneiro, F. B. Rasmussen, M. Olsen, G. Rindorf, C. S. Jacobsen, H. J. Pedersen, J. C. Scott, *J. Am. Chem. Soc.* **1981**, *103*, 2440-2442.

[20] a) I. Fernandez-Torrente, S. Monturet, K. J. Franke, J. Fraxedas, N. Lorente, J. I. Pascual, *Phys. Rev. Lett.* **2007**, *99*, 176103/1-176103/4; b) J. Fraxedas, S. Garcia-Gil, S. Monturet, N. Lorente, I. Fernandez-Torrente, K. J. Franke, J. I. Pascual, A. Vollmer, R. P. Blum, N. Koch, P. Ordejon, *J. Phys. Chem. C* **2011**, *115*, 18640-18648.

[21] a) J. Fraxedas, *Molecular Organic Materials: From Molecules to Crystalline Solids*, Cambridge University Press, Cambridge, UK, **2006**; b) G. Subias, T. Abbaz, J. M. Fabre, J. Fraxedas, *Phys. Rev. B: Condens. Matter Mater. Phys.* **2007**, *76*, 085103/1-085103/7.

[22] a) J. Fraxedas, Y. J. Lee, I. Jimenez, R. Gago, R. M. Nieminen, P. Ordejon, E. Canadell, *Phys. Rev. B: Condens. Matter Mater. Phys.* **2003**, *68*, 195115/1-195115/11; b) M. Sing, U. Schwingenschlogl, R. Claessen, M. Dressel, C. S. Jacobsen, *Phys. Rev. B: Condens. Matter Mater. Phys.* **2003**, *67*, 125402/1-125402/11.

[23] R. Bozio, C. Pecile, K. Bechgaard, F. Wudl, D. Nalewajek, *Solid State Communications* **1982**, *41*, 905-910.

[24] D. U. Gubser, W. W. Fuller, T. O. Poehler, D. O. Cowan, M. Lee, R. S. Potember, L. Y. Chiang, A. N. Bloch, *Phys. Rev. B J1 - PRB* **1981**, *24*, 478-480.

[25] L. E. Winter, E. S. Steven, J. S. Brooks, D. de Caro, C. Faulmann, L. Valade, K. Jacob, I. Chtioui, J. Fraxedas, B. Ballesteros, to be published.

[26] G. Steimecke, H.-J. Sieler, R. Kirmse, E. Hoyer, *Phosphorus and Sulfur* **1979**, *7*, 49-55.

[27] M. Bergez-Lacoste, S. Thiebaud-Roux, P. de Caro, J.-F. Fabre, Z. Mouloungu, *Dérivés du furfural pour une application biosolvants*,Patent FR1351811, France, **2013**

[28] a) P. Cassoux, L. Valade, P.-L. Fabre, in *Comprehensive Coordination Chemistry II: From Biology to Nanotechnology, Fundamentals: ligands, Complexes, Synthesis, Purification and Structure, Vol. 1* (Ed.: A. B. P. Lever), Elsevier, Amsterdam, **2003**, pp. 761-773; b) P. Batail, K. Boubekeur, M. Fourmigué, J.-C. P. Gabriel, *Chem. Mater.* **1998**, *10*, 3005-3015.